Implementation Schemes to Compensate for Inverter Nonlinearity Based on Trapezoidal Voltage

Yongsoon Park, *Student Member, IEEE*, and Seung-Ki Sul, *Fellow, IEEE*

***Abstract*—Trapezoidal voltages can be used to compensate for the inverter nonlinearity. In particular, the modulating shape of these voltages facilitates the adaptation of the compensation to various operating conditions. In this paper, practical implementation schemes are proposed to improve the performance of the compensation method based on the trapezoidal voltage. After the implementation schemes are detailed, their effectiveness is discussed with experimental results. It has been proved that the proposed schemes are useful for the robust compensation.**

***Index Terms*—Inverter nonlinearity, permanent-magnet synchronous motor (PMSM), sensorless control, trapezoidal voltage.**

I. Introduction

VOLTAGE-SOURCE inverters are commonly used for power conversions such as ac motor drives and grid-tied applications. The switches used in the inverter must be controlled so that two terminals of a dc-link capacitor are not directly connected to each other. Thus, when a pair of switches operates complementarily, their turn-on instants are intentionally delayed by a certain time, which is so called as dead time. This dead time causes distortions in output voltages [1], [2]. Moreover, the varying slopes of output voltages at turn-on/turn-off are limited [3]–[7] and affected by parasitic components in the current paths [8]–[11]. That is, actual outputs of an inverter may be different from the corresponding voltage references due to the inverter's practical characteristics.

This type of nonlinearity can result in harmonic currents. Because load power is mainly transferred via fundamental currents, the other harmonics are undesirable losses unless they are exploited for a special purpose [12]. The harmonic currents also represent torque ripples and may result in speed ripples if the motor inertia is small. In addition, since voltage references may be different from actual outputs, the estimation of motor parameters would not be accurate if these differences are not offset [13].

For the last few decades, it has been discussed how the nonlinearity of an inverter can be offset [1]–[11]. Even though diverse discussions have been developed, it might be still a challenging issue to ensure the effectiveness of a compensation method for a wide operating range. Among several attempts to compensate for the inverter nonlinearity, a method utilizing trapezoidal voltages was proposed to enable adaptive compensations to various operating conditions [14], [15]. In this method, the shape of trapezoidal voltages, which are added to pole voltage references, is modified in real time depending on operating conditions. The harmonic voltages incorporated in the trapezoidal voltages can then be adjusted toward mitigating harmonic currents. Through the comparisons to the other compensation methods, it had been presented that the compensation method based on trapezoidal voltages could outperform the others even if operating conditions were changed.

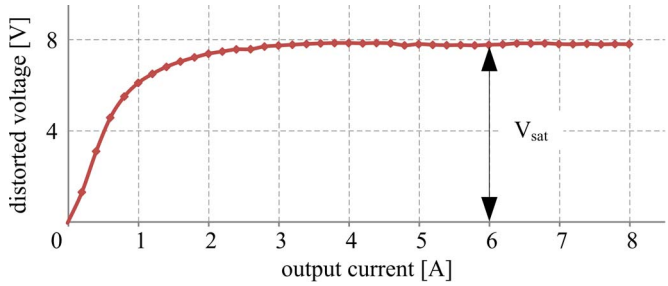

Fig. 1. Estimated distortion of an inverter at standstill.

In this paper, the compensation method based on the trapezoidal voltage is further improved. In Section II, useful implementation schemes for the compensation are proposed. After the tuning effect of the trapezoidal voltage is examined in the view point of harmonic voltages, it is discussed which harmonics should be critically taken into account for the compensation. An additional scheme is discussed to enhance the transient dynamics of the compensation method. In Section III, the effectiveness of the proposed schemes is assessed via experimental results obtained from practical systems driving permanent-magnet synchronous motors (PMSMs). To confirm evident effects of the proposed method, the PMSMs were driven by a sensorless control method [18]. While the conventional method had been only tested at ordinary load conditions, the proposed method was demonstrated at more extreme load conditions. The conclusions are then given in Section IV.

II. Implementation Schemes for Compensation

A. Harmonics of Trapezoidal Voltage

The distorted voltage due to the inverter nonlinearity can be estimated when a motor is at standstill [10], [15]. Fig. 1 presents the estimated distortions with respect to output currents in a

Manuscript received October 17, 2012; revised March 28, 2013; accepted June 5, 2013. Date of publication July 4, 2013; date of current version March 17, 2014. Paper 2012-IDC-574.R1, presented at the 2012 IEEE Energy Conversion Congress and Exposition, Raleigh, NC, USA, September 15–20, and approved for publication in the IEEE Transactions on Industry Applications by the Industrial Drives Committee of the IEEE Industry Applications Society.

The authors are with Seoul National University, Seoul 151-744, Korea (e-mail: yongsoon@eepel.snu.ac.kr; sulsk@plaza.snu.ac.kr).

Color versions of one or more of the figures in this paper are available online at http://ieeexplore.ieee.org.

Digital Object Identifier 10.1109/TIA.2013.2272431

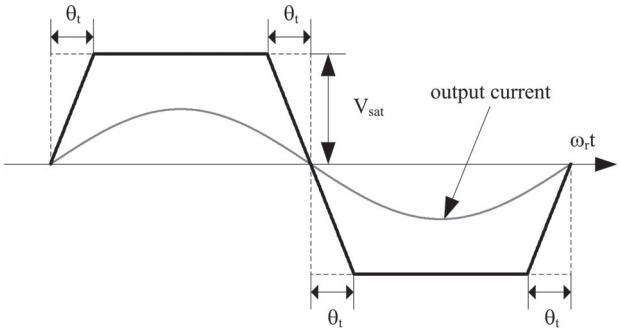

Fig. 2. Definition of trapezoidal voltage.

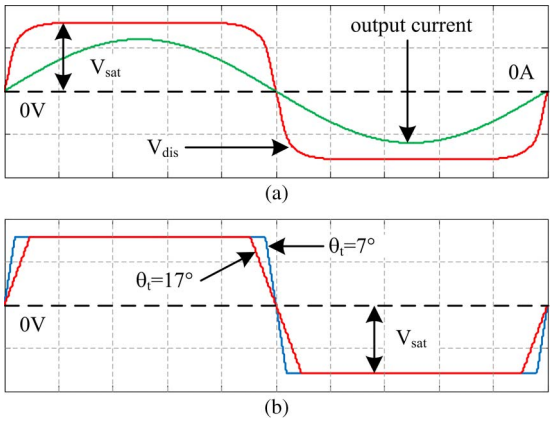

Fig. 3. (a) Output current and estimated voltage distortion ($V_{\rm dis}$) and (b) trapezoidal voltages (current: 5 A/div; voltage: 5 V/div; and time: 10 ms/div).

prototype inverter [15]. Several studies have shown that this type of distortion shape can be exploited for the compensation [8]–[11]. Namely, when one of output currents is sampled, the compensation is carried out such that its corresponding voltage in Fig. 1 is fed forward to the pole voltage reference of the same phase. The negative current case is treated symmetrically.

The idea to utilize a trapezoidal voltage arises from the first-order linear approximation of the voltage variations in the current range up to the saturation. The trapezoidal voltage was depicted in Fig. 2. By adjusting the trapezoidal angle θ_t, the compensation voltage can be a square waveform or a triangular waveform. This trapezoidal angle should be determined so that the compensation becomes appropriate for given operating conditions.

Based on Fig. 1, the distorted voltage due to the inverter nonlinearity could be estimated as $V_{\rm dis}$ in Fig. 3(a) when the output current's peak was 6 A and its frequency was 10 Hz. Although it might be controversial how much accurate the estimated distortion is, it has been shown that this distortion is effective enough for the compensation [8]–[11].

Several trapezoidal voltages with different trapezoidal angles can be the approximate candidates to substitute for $V_{\rm dis}$. For example, the trapezoidal voltages whose trapezoidal angles are 7° and 17°, respectively, were depicted in Fig. 3(b). It is plausible that one of trapezoidal angles between 7° and 17° can be selected for the suitable approximation. This selection can be based on frequency analysis. Because $V_{\rm dis}$ and the trapezoidal voltage are periodic and symmetric to the zero crossings, each

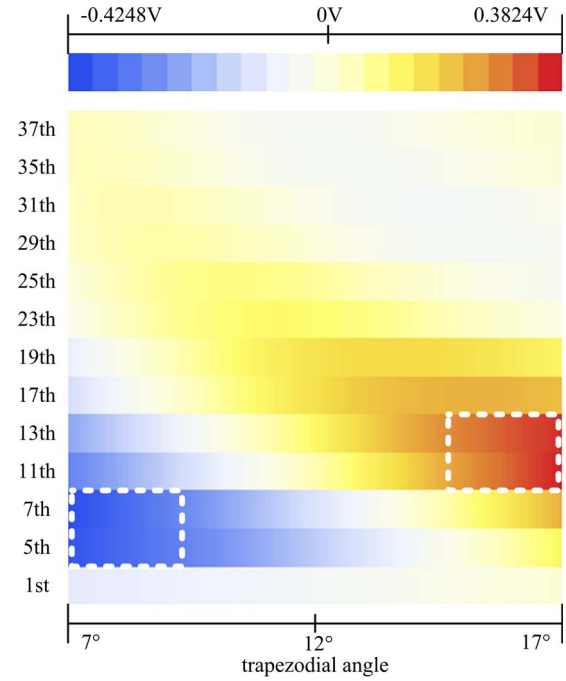

Fig. 4. Error function of Fourier coefficients according to trapezoidal angle.

voltage can be described with the Fourier series whose even harmonics and cosine terms are disregarded. Moreover, when the motor driven by the inverter is a Y-connected three-phase type, the harmonics that are multiples of three can be ignored as well.

With respect to the harmonics of interest, an error function between the Fourier coefficients can be defined as

$$e^n_{\rm coeff} = a^n_{\rm dis} - a^n_{\rm trape} \tag{1}$$

where the superscript "n" represents the harmonic order. The subscript "dis" means the estimated distortion, and "trape" refers to the trapezoidal voltage. The unit of the error function is volt.

When the trapezoidal angle was changed by 0.1° from 7° to 17°, the error function in (1) was calculated. The calculated results are shown in Fig. 4. Within the angle range, the coefficient errors for the fundamental one were trivial. This is almost the same for the higher order harmonics. However, as indicated by the dashed boxes in Fig. 4, the 5th, 7th, 11th, and 13th harmonics present relatively large deviations. That is, when compared to the estimated distortion, those harmonics of trapezoidal voltage are mainly changed according to the variation of the trapezoidal angle.

To quantify the degree of the coefficient deviations, the following indicator can be defined:

$$I^{\theta_t}_{\rm err} = \sqrt{\sum_n \left(e^n_{\rm coeff}\right)^2} \tag{2}$$

where n can be 1, 5, 7, 11, 13, 17, 19, 23, 25, 29, 31, 35, and 37. The superscript "θ_t" represents a trapezoidal angle.

By finding the trapezoidal angle minimizing the deviation indicator of (2), the trapezoidal voltage well matched to the

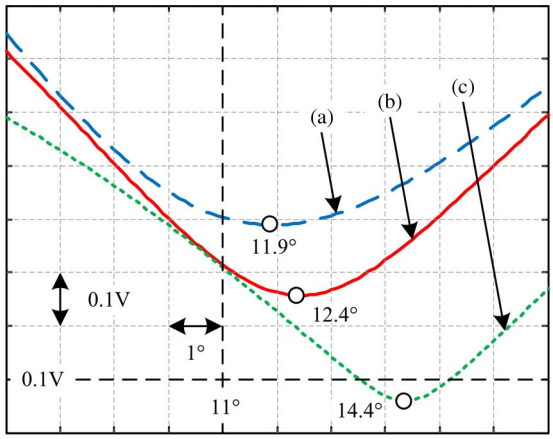

Fig. 5. Coefficient deviation indicator when harmonic orders of concern are (a) from 1 to 37, (b) from 5 to 13, and (c) from 5 to 7.

estimated distortion can be selected. As shown in Fig. 5, 11.9° is the optimal angle when up to the 37th harmonics are considered. Given that the deviations of the high-order harmonics are not dominant, as shown in Fig. 4, the deviation indicator can be approximated by considering low-order harmonics only. It is shown in Fig. 5 that the trapezoidal angle to generate the minimum indicator considering the 5th, 7th, 11th, and 13th harmonics is closer to the optimal one than that considering the fifth and seventh harmonics. It is evident that the trapezoidal angle can be differently determined depending on the harmonic orders of interest.

B. Modulation of Trapezoidal Angle

Since the data in Fig. 1 are normally obtained at one operating point, the estimated distortion based on Fig. 1 may not be accurate at the other operating points. Therefore, the indicator in (2) could not be sufficient to appropriately determine the trapezoidal angle for a wide operating range. Instead, harmonics in output currents can be fed back to determine the trapezoidal angle if the harmonic currents are dominantly caused by the inverter nonlinearity.

A coordinate transformation can be helpful to observe the harmonic currents [14], [15]. For the transformation, the current angle of the a phase, denoted by θ_a, can be defined such that $\sin\theta_a$ is in phase with the a-phase current of i_{as}, as shown in Fig. 6. In particular, the angle range between $-\pi$ and π is desirable to synthesize a trapezoidal voltage.

After θ_t and $V_{\rm sat}$ in Fig. 2 are determined, the following slope can be calculated:

$$S_{\rm trape} = V_{\rm sat}/\theta_t. \tag{3}$$

Synthesizing a trapezoidal voltage is only detailed within the positive range of θ_a because the negative range is just symmetric. Considering θ_t in Fig. 2, the positive range of θ_a can be divided into

$$0 \le \theta_a < \theta_t \tag{4}$$

$$\theta_t \le \theta_a < \pi - \theta_t \tag{5}$$

$$\pi - \theta_t \le \theta_a < \pi. \tag{6}$$

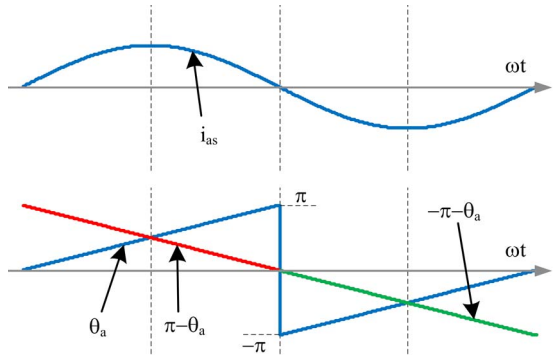

Fig. 6. a-phase current (i_{as}) and its angle (θ_a).

In the range of (5), the trapezoidal voltage is simply equal to $V_{\rm sat}$ as per Fig. 2. If θ_a is within (4), the trapezoidal voltage can be calculated through multiplying θ_a by $S_{\rm trape}$ in (3). Considering the variation of $\pi - \theta_a$ in Fig. 6, the trapezoidal voltage with (6) can be calculated through multiplying $\pi - \theta_a$ by $S_{\rm trape}$.

Since the current angle may be different from the rotor flux angle, the q-axis current in the frame synchronized with the current angle should be calculated through a separate coordinate transformation [14]. However, currents in the stationary $d-q$ reference frame are usually computed by the Clarke transformation for normal current controls, not only for the compensation method

$$\begin{cases} i_{ds}^s = i_{as} \\ i_{qs}^s = (i_{bs} - i_{cs})/\sqrt{3} \end{cases} \tag{7}$$

where the superscript "s" represents the stationary reference frame.

Then, if the current angle θ_a is given, the q-axis current can be obtained by

$$i_{qs}^a = \cos\theta_a \cdot i_{ds}^s + \sin\theta_a \cdot i_{qs}^s \tag{8}$$

where the superscript "a" represents the reference frame synchronized with the current angle θ_a.

The fifth and seventh harmonic currents are merged into a sixth-order harmonic in the synchronously rotating reference frame [14], [15]. Likewise, the 11th and 13th harmonics are merged into a 12th-order harmonic. In the conventional method, only the sixth-order harmonic in the synchronous frame was considered to modulate the trapezoidal angle. However, as discussed in Figs. 4 and 5, the 11th- and 13th-order harmonics in a trapezoidal voltage may result in evident effects on the compensation. Therefore, to reflect these harmonics additionally, the modulator for the trapezoidal angle has been modified, as shown in Fig. 7. Namely, the part pertaining to $\sin(12\theta_a)$ has been newly proposed when compared to the conventional method. In Fig. 7, the parts denoted by "LPF" indicate low-pass filtering. Each "LPF" was implemented with the second-order filter, whose bandwidth was set at 3 Hz.

In particular, the switch denoted by "SW" in Fig. 7 is considered in the modulator operation. The SW is closed only if θ_t is smaller than 15°. This is because 11th- and 13th-order harmonics of trapezoidal voltage are not monotonically

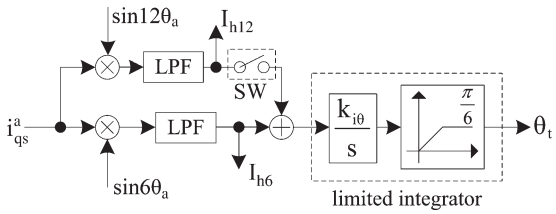

Fig. 7. Modulator for trapezoidal angle.

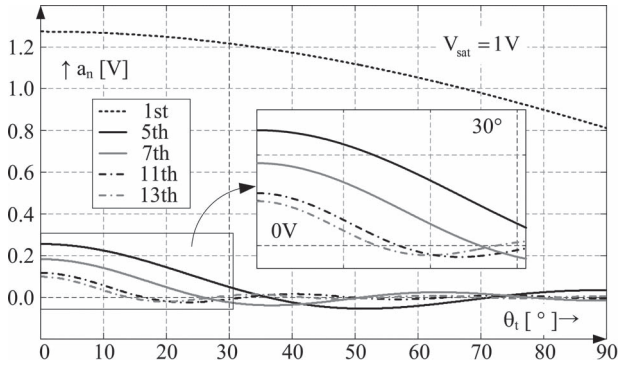

Fig. 8. Fourier coefficients of 1st, 5th, 7th, 11th, and 13th harmonics according to trapezoidal angle.

changed by θ_t over 15°, as shown in Fig. 8. Namely, the 11th- and 13th-order harmonic currents are considered in determining the trapezoidal angle only if the integrator action is effective to modulate those harmonics of trapezoidal voltage.

C. Detection of Current Angle

As described in the previous section, the current angle is essential for the compensation. In the conventional method, a three-phase phase-locked loop (PLL) was used to detect the current angle [16], [17].

However, the estimated current angle can include some errors during transients due to the limited dynamics of the PLL. Then, the compensation based on the PLL can be impeded if output currents are needed to be changed under sudden load variations. Moreover, the phase locking would be effective only if the locked signal is large enough. That is, if output currents are very small, the current angle might not be detected.

The trapezoidal angle is normally set to a definite value. However, if the current angle is not clearly detected, the shape of the trapezoidal voltage can be crushed. Furthermore, the input to the modulator in Fig. 7 may be distorted if the coordinate transformation is contaminated by some angle distortions. Therefore, without a robust method to clearly detect current angles, the adaptiveness of the compensation cannot be ensured for a wide operating range.

To improve the angle detection, information of current references can be utilized. In a steady state, output currents coincide with their references by virtue of feedback controls. Otherwise, voltage references in the synchronous reference frame would be further modified by the feedback loops to counterbalance the current errors. Because these voltage variations contradict the assumption of the steady state, the current should be identical

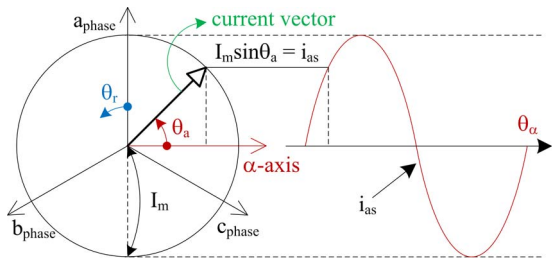

Fig. 9. Current vector and a-phase current.

to its reference. That is, the reference information can be used for the angle detection.

By the Clarke transformation, a three-phase current can be transformed into the current vector that rotates at a synchronous speed in the stationary reference frame. When the rotor angle, defined as θ_r in Fig. 9, is considered, the angular position of a current vector can be derived as

$$\theta_i = \theta_r + \text{atan2}\left(i_{qs}^{r^*}, i_{ds}^{r^*}\right) \tag{9}$$

where the superscript "r" represents the rotor reference frame and the reference values are indicated by the superscript "*." The function of atan2 is a variation of the arctangent function [22].

As per its definition, it can be inferred that θ_a starts from the α-axis leading the a-phase axis by 90°, as depicted in Fig. 9. That is, θ_a is zero when the current vector is aligned with the α-axis. This alignment occurs when θ_i in (9) is equal to $3\pi/2$. Additionally, when the derivative of each angle is considered, the current angle θ_a can be derived as (10) in terms of θ_r

$$\theta_a = \theta_r + \text{atan2}(i_{qs}^{r^*}, i_{ds}^{r^*}) - 1.5\pi. \tag{10}$$

Of course, to synthesize trapezoidal voltages, θ_a in (10) may have to be further processed so that it is between $-\pi$ and π. The current angle obtained by (10) has two features. One is that its detection is at least not delayed. The other is that harmonic distortions possibly incorporated in output currents less affect the angle detection. How these features would be helpful for the compensation is confirmed with experimental results in the next section.

III. Experiments

A. Experimental Setups

To demonstrate the proposed method, practical driving systems were used. The test motors were a surface-mounted PMSM (SMPMSM) and an interior PMSM (IPMSM) shown in Fig. 10. The ratings of the SMPMSM are 1500 r/min and 11.5 N · m, and those of the IPMSM are 5400 r/min and 9 N · m. The pole pairs of the SMPMSM and the IPMSM are four and two, respectively. Both motors were driven by a sensorless control method [18]. In addition, the dc-link voltage of the inverter was supplied via a diode rectifier connected to a $3\phi 220$-V_{rms} source for SMPMSM, and this composition was the same for IPMSM with a 380-V_{rms} source.

All control algorithms were implemented in the same control board based on TMS320VC33. The pulsewidth modulation

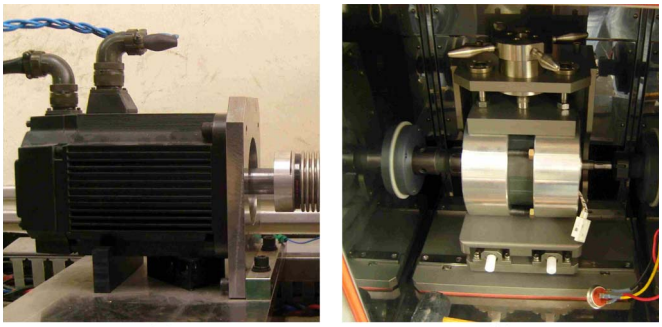

(a) (b)

Fig. 10. Test motors: (a) SMPMSM and (b) IPMSM.

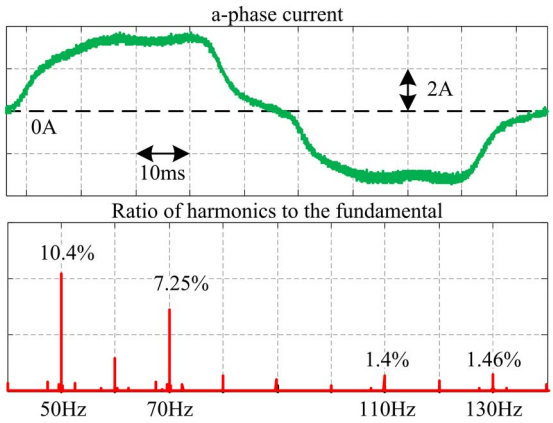

Fig. 11. Output current and its FFT without any compensation.

(PWM) was based on space vector PWM [20]. The sampling period was set to 100 μs; the switching period was set to 200 μs. Although the dead time was identically set to 3 μs for each inverter, the saturated voltages, $V_{\rm sat}$ in Fig. 2, were measured according to the measuring procedure in [15] as 5.56 V for the inverter driving SMPMSM and 7.88 V for the inverter driving IPMSM. This is because the different dc-link voltages cause the different volt–second distortions even under the same dead time [1]. However, the integral gain $k_{i\theta}$ for both inverters was set to 20, which was empirically determined.

B. Experimental Results

Initially, the compensation effect of mitigating harmonics in output currents was considered. The SMPMSM was driven at 150 r/min, which corresponds to 10 Hz in electrical speed, under 1.5-N · m load. To present obvious differences, fast Fourier transform (FFT) was applied to output currents that were measured for 100 s under 50-kHz samplings through a current probe. For comparison, the result without any compensation was presented in Fig. 11.

As a distortion indicator, selective harmonic distortion (SHD) can be defined as

$$\mathrm{SHD}[\%] = \frac{\sqrt{I_5^2 + I_7^2 + I_{11}^2 + I_{13}^2}}{I_1} \times 100 \qquad (11)$$

where I_n refers to a current magnitude at the nth-order harmonic.

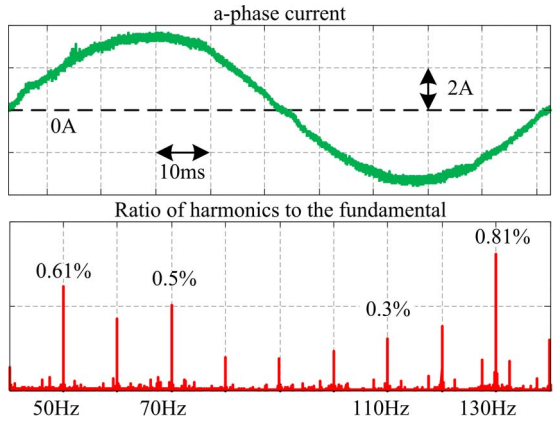

Fig. 12. Output current and its FFT when fifth- and seventh-order harmonics were considered to modulate trapezoidal angle.

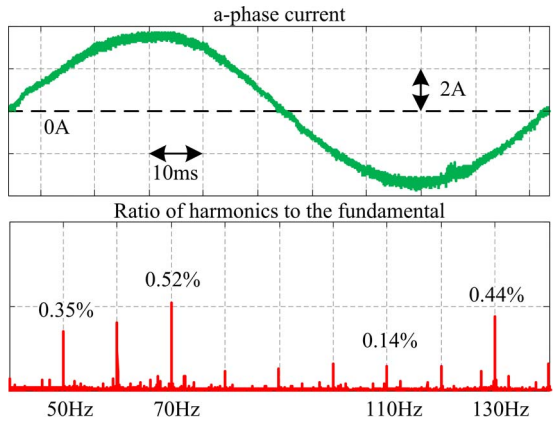

Fig. 13. Output current and its FFT when 5th-, 7th-, 11th-, and 13th-order harmonics were considered to modulate trapezoidal angle.

Then, the SHD in the case of Fig. 11 was computed as 12.8%. This indicates that the output current is severely distorted. With the conventional method considering only the fifth- and seventh-order harmonics, harmonic currents were evidently mitigated as shown in Fig. 12. In this case, the SHD was 1.17%, which is less than one-tenth of that in Fig. 11.

Although the compensation effect was excellent with the conventional method, the harmonic characteristics can be more improved with the proposed method. The result by the proposed method is shown in Fig. 13. Compared with those in Fig. 12, the 11th- and 13th-order harmonic currents were more reduced, while the currents of the fifth and seventh harmonics remained similar. This is because the 11th and 13th harmonics were taken into account to modulate the trapezoidal angle. The SHD with the proposed method was 0.78%.

The operational difference between the conventional and the proposed methods can be explained with Fig. 14. The trapezoidal angles determined by the conventional and the proposed methods were 11.46° and 10.14°, respectively. Another difference in each case was the magnitude of the harmonic currents defined as I_{h6} and I_{h12} in Fig. 7.

In the conventional method, because only I_{h6} is considered, the trapezoidal angle θ_t converges toward minimizing the sixth-order harmonic in the synchronous reference frame, as shown

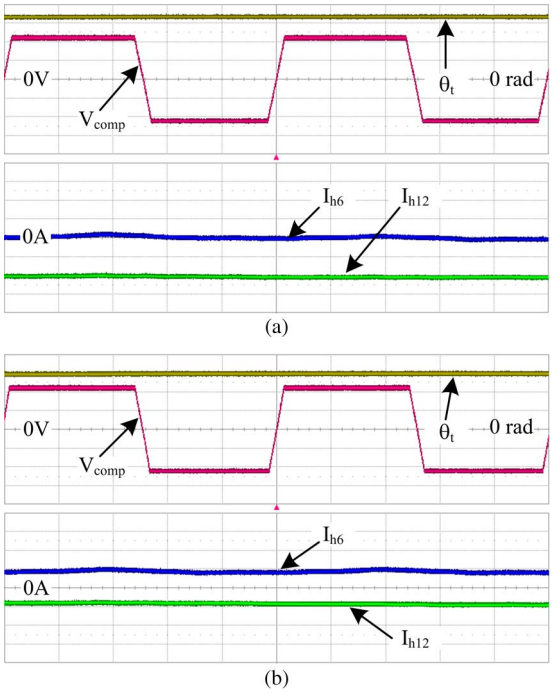

Fig. 14. Harmonic currents and trapezoidal voltage with (a) conventional method and (b) proposed method ($V_{\rm comp}$: 2.5 V/div; θ_t: 0.06 rad/div; I_{h6} and I_{h12}: 10 mA/div; and time: 20 ms/div).

in Fig. 14(a). That is, the modulator for θ_t does not contribute to minimizing the 12th harmonic at the same time.

By contrast, in the proposed method, I_{h6} and I_{h12} are considered simultaneously. The trapezoidal angle is then adjusted toward minimizing the sum of those currents, as shown in Fig. 14(b). This feature can contribute to evenly mitigating the harmonic currents. In particular, even in the proposed method, the 11th- and 13th-order harmonic currents are reflected for the compensation only if the trapezoidal angle is less than 15°. However, within this angle range, magnitude variations of the fifth- and seventh-order harmonics by θ_t are relatively small, as shown in Fig. 8. That is, the compensation effects on the 11th- and 13th-order harmonics can be improved, while those on the fifth- and seventh-order harmonics remain similarly. This is corroborated with Figs. 12 and 13.

Although SMPMSMs are operated with the d-axis current regulated as null, this is not the case for IPMSMs. When the d-axis current of the IPMSM in the rotor reference frame was regulated as -1.5 A, the compensation results are presented in Fig. 15. After the trapezoidal voltage of $V_{\rm comp}$ was applied during driving, the driving performance was improved in two aspects.

First, harmonic currents were mitigated like the case of SMPMSM. Namely, the d–q currents in the stationary reference frame became closer to sine waves. Second, the rotor angle error in the sensorless control, which was denoted by $\theta_r - \hat{\theta}_r$ in Fig. 15, decreased. This is because the fundamental distortions in voltage references caused by the inverter nonlinearity were offset by the compensation method based on the trapezoidal voltage simultaneously [21]. This type of angle error compensation is not possible by harmonic controllers such as resonant

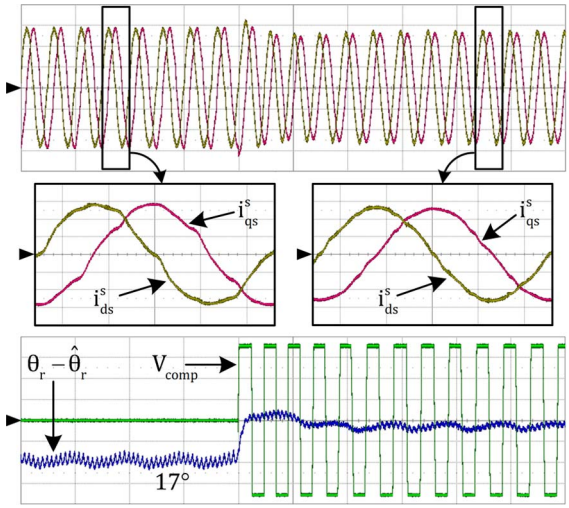

Fig. 15. Compensation effects under a nonzero d-axis current, 300 r/min, and 2-N · m load (currents: 2 A/div with center at 0 A; $V_{\rm comp}$: 2.5 V/div with center at 0 V; $\theta_r - \hat{\theta}_r$: 0.15 rad/div with center at 0 rad; and time: 200 ms/div).

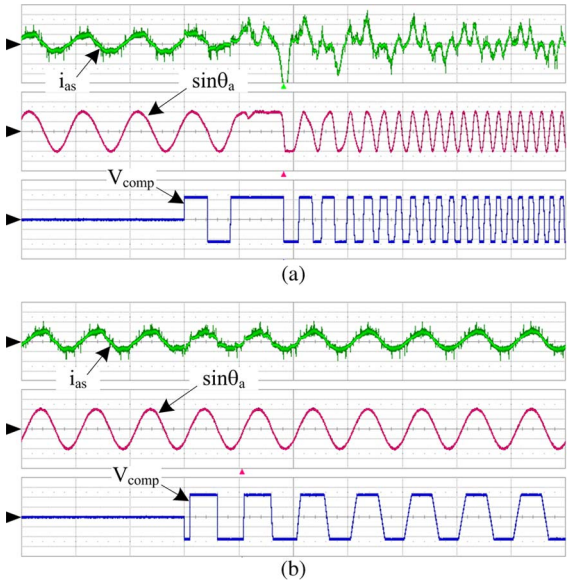

Fig. 16. Compensation effects at 150 r/min with no load when current angle is detected by (a) PLL method and (b) proposed method (i_{as}: 1 A/div with center at 0 A; sin θ_a: 0.5/div with center at zero; $V_{\rm comp}$: 2.5 V/div with center at 0 V; and time: 100 ms/div).

controllers [19], which do not focus on offsetting the fundamental voltage distortion.

In the aforementioned experimental results, the current angle had been detected by using the current references because the analyses were mainly concentrated on steady states. The effectiveness of the reference-based angle detection is examined with the following experimental results. For these experiments, the proposed modulator in Fig. 7 was commonly used.

To compare the effects of each angle detection method, the SMPMSM was driven at 150 r/min with no load. Before the trapezoidal voltages were applied for the compensation, it could be recognized that θ_a was well detected even by the PLL, as shown in Fig. 16(a). However, after the compensation started, the PLL lost its detection ability, whereas the proposed method

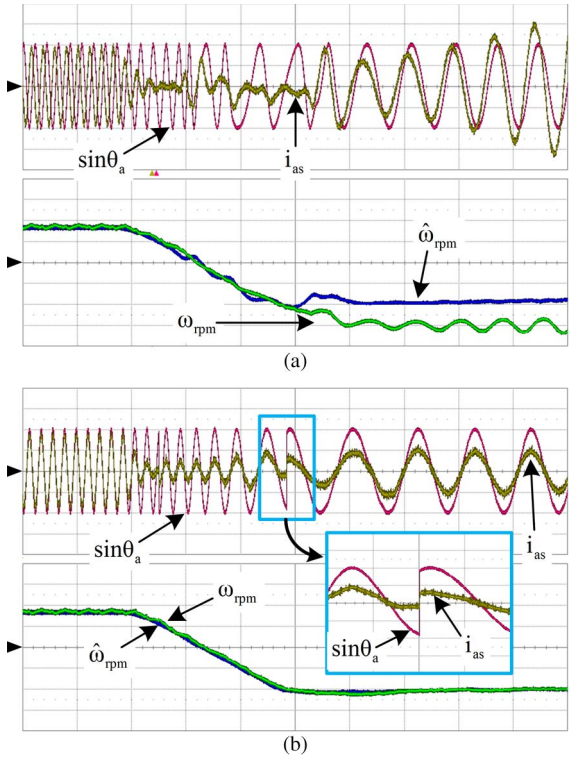

Fig. 17. Compensation effects under deceleration of the speed when using (a) PLL method and (b) proposed method (i_{as}: 1 A/div with center at 0 A; $\sin\theta_a$: 0.5/div with center at zero; $\omega_{\rm rpm}$ and $\hat{\omega}_{\rm rpm}$: 150 r/min/div with center at 450 r/min; and time: 200 ms/div).

based on the current references did not. At this operating point, the back electromotive force was expected to be 6.35 $V_{\rm peak}$, while the peak value of the trapezoidal voltage was 5.56 V. That is, when voltage references are relatively small, output currents are vulnerable to distortions even from applying trapezoidal voltages. Furthermore, because the filtering effect on distortions cannot be perfect in the PLL-based method, the compensation can fail, as shown in Fig. 16(a). However, the proposed method could be effective, as shown in Fig. 16(b), because current references used for the angle detection were less affected by distortions.

Each compensation method was also tested at a varying operating condition, where the speed of the IPMSM was decelerated from 700 to 150 r/min under no load. This condition has been considered as the worst case because both frequency and magnitude of output currents are decreasing. Furthermore, the d–q current references in the synchronously rotating reference frame can be changed in a step manner to follow torque references under this condition. In fact, the current angle estimated by the PLL cannot be changed abruptly due to its low-pass filtering [16]. This shortcoming even led to instability of the sensorless operation, as shown in Fig. 17(a). Namely, the estimated speed $\hat{\omega}_{\rm rpm}$ had deviated from the actual speed $\omega_{\rm rpm}$. Finally, the entire control system had to be stopped by an overcurrent protection at standstill.

When output currents are still converging to their references, it can be ambiguous where the current vector is located. Moreover, the detection of the current angle cannot help being delayed due to the PLL's limited dynamics. Unlike the PLL-based method, the predicted current angles at which output currents should be located are used in the proposed method. In addition, step variations of the current angle can be tracked in the detection method based on the references. As enlarged in Fig. 17(b), the estimated current angle could be changed by almost 180° in the practical implementation of the proposed method. Only by changing the angle detection scheme, the sensorless operation combined with the compensation remained normal during and after the deceleration. This improvement was achieved by the proposed scheme.

IV. Conclusion

To compensate for the inverter nonlinearity, the compensation principles based on trapezoidal voltages had already been explained in the literature. In this paper, practical schemes to implement the compensation method have been further proposed for better performances under diverse operating conditions. By the proposed schemes, harmonic distortions caused by the inverter nonlinearity could be more mitigated, and the stability of the driving system with a sensorless control method could be enhanced. Therefore, these sorts of improvements would contribute to the enhancement of the adaptive feature in the compensation method using the trapezoidal voltage.

References

[1] Y. Murai, T. Watanabe, and H. Iwasaki, "Waveform distortion and correction circuit for PWM inverters with switching lag-times," *IEEE Trans. Ind. Appl.*, vol. IA-23, no. 5, pp. 881–886, Sep. 1987.
[2] D. Leggate and R. J. Kerkman, "Pulse-based dead-time compensator for PWM voltage inverters," *IEEE Trans. Ind. Electron.*, vol. 44, no. 2, pp. 191–197, Apr. 1997.
[3] J.-W. Choi and S.-K. Sul, "Inverter output voltage synthesis using novel dead time compensation," *IEEE Trans. Power Electron.*, vol. 11, no. 2, pp. 221–227, Mar. 1996.
[4] A. R. Munoz and T. A. Lipo, "On-line dead-time compensation technique for open-loop PWM-VSI drives," *IEEE Trans. Power Electron.*, vol. 14, no. 4, pp. 683–689, Jul. 1999.
[5] H.-S. Kim, H.-T. Moon, and M.-J. Youn, "On-line dead-time compensation method using disturbance observer," *IEEE Trans. Power Electron.*, vol. 18, no. 6, pp. 1336–1345, Nov. 2003.
[6] H. Zhao, J. Wu, and A. Kawamura, "An accurate approach of nonlinearity compensation for VSI inverter output voltage," *IEEE Trans. Power Electron.*, vol. 19, no. 4, pp. 1029–1035, Jul. 2004.
[7] S.-H. Hwang and J.-M. Kim, "Dead time compensation method for voltage-fed PWM inverter," *IEEE Trans. Energy Convers.*, vol. 25, no. 1, pp. 1–10, Mar. 2010.
[8] L. M. Gong and Z. Q. Zhu, "A novel method for compensating inverter nonlinearity effects in carrier signal injection-based sensorless control from positive-sequence carrier current distortion," *IEEE Trans. Ind. Appl.*, vol. 47, no. 3, pp. 1283–1292, May/Jun. 2011.
[9] N. Urasaki, T. Senjyu, T. Kinjo, T. Funabashi, and H. Sekine, "Dead-time compensation for permanent magnet synchronous motor drive taking zero-current clamp and parasitic capacitance effects into account," *Proc. Inst. Elect. Eng.—Elect. Power Appl.*, vol. 152, no. 4, pp. 845–853, Jul. 8, 2005.
[10] G. Pellegrino, R. I. Bojoi, P. Guglielmi, and F. Cupertino, "Accurate inverter error compensation and related self-commissioning scheme in sensorless induction motor drives," *IEEE Trans. Ind. Appl.*, vol. 46, no. 5, pp. 1970–1978, Sep./Oct. 2010.
[11] S. Bolognani, L. Pretti, and M. Zigliotto, "Repetitive-control-based self-commissioning procedure for inverter nonidealities compensation," *IEEE Trans. Ind. Appl.*, vol. 44, no. 5, pp. 1587–1596, Sep./Oct. 2008.
[12] Y.-D. Yoon, S.-K. Sul, S. Morimoto, and K. Ide, "High-bandwidth sensorless algorithm for AC machines based on square-wave-type voltage injection," *IEEE Trans. Ind. Appl.*, vol. 47, no. 3, pp. 1361–1370, May/Jun. 2011.

[13] Y. Inoue, K. Yamada, S. Morimoto, and M. Sanada, "Effectiveness of voltage error compensation and parameter identification for model-based sensorless control of IPMSM," *IEEE Trans. Ind. Appl.*, vol. 45, no. 1, pp. 213–221, Jan./Feb. 2009.
[14] Y. Park and S.-K. Sul, "A novel method to compensate non-linearity of inverter in sensorless operation of PMSM," in *Proc. 8th IEEE ICPE-ECCE*, May 30/Jun. 3, 2011, pp. 915–922.
[15] Y. Park and S.-K. Sul, "A novel method utilizing trapezoidal voltage to compensate for inverter nonlinearity," *IEEE Trans. Power Electron.*, vol. 27, no. 12, pp. 4837–4846, Dec. 2012.
[16] S.-K. Chung, "A phase tracking system for three phase utility interface inverter," *IEEE Trans. Power Electron.*, vol. 15, no. 3, pp. 431–438, May 2000.
[17] F. D. Jreijedo, A. G. Yepes, O. Lopez, A. Vidal, and J. Doval-Gandoy, "Three-phase PLLs with fast postfault retracking and steady-state rejection of voltage unbalance and harmonics by means of lead compensation," *IEEE Trans. Power Electron.*, vol. 26, no. 1, pp. 85–97, Jan. 2011.
[18] B.-H. Bae, S.-K. Sul, J.-H. Kwon, and J.-S. Byeon, "Implementation of sensorless vector control for super-high speed PMSM of turbo-compressor," *IEEE Trans. Ind. Appl.*, vol. 39, no. 3, pp. 811–818, May/Jun. 2003.
[19] R. Teodorescu, F. Blaabjerg, M. Liserre, and P. C. Loh, "Proportional-resonant controllers and filters for grid-connected voltage-source converters," *Proc. Inst. Elect. Eng.—Elect. Power Appl.*, vol. 153, no. 5, pp. 750–762, Sep. 2006.
[20] D.-W. Chung, J.-S. Kim, and S.-K. Sul, "Unified voltage modulation technique for real-time three-phase power conversion," *IEEE Trans. Ind. Appl.*, vol. 34, no. 2, pp. 374–380, Mar./Apr. 1998.
[21] Y. Park, S.-K. Sul, J.-K. Ji, and Y.-J. Park, "Analysis of estimation errors in rotor position for a sensorless control system using a PMSM," *J. Power Electron.*, vol. 12, no. 5, pp. 748–757, Sep. 2012.
[22] A. Ukil, V. H. Shah, and B. Deck, "Fast computation of arctangent functions for embedded applications: A comparative analysis," in *Proc. IEEE ISIE*, Jun. 27–30, 2011, pp. 1206–1211.

Yongsoon Park (S'12) received the B.S. and M.S. degrees in electrical engineering from Seoul National University, Seoul, Korea, in 2008 and 2010, respectively, where he is currently working toward the Ph.D. degree.

His current research interests include sensorless drives of electrical machines and power conversion circuits.

Seung-Ki Sul (S'78–M'80–SM'98–F'00) received the B.S., M.S., and Ph.D. degrees in electrical engineering from Seoul National University, Seoul, Korea, in 1980, 1983, and 1986, respectively.

From 1986 to 1988, he was an Associate Researcher with the Department of Electrical and Computer Engineering, University of Wisconsin, Madison, WI, USA. From 1988 to 1990, he was a Principal Research Engineer with Gold-Star Industrial Systems Company. Since 1991, he has been a member of the faculty of the School of Electrical Engineering, Seoul National University, where he was the Vice Dean of the Engineering College from 2005 to 2007, was the President of the Korea Electrical Engineering and Science Research Institute from 2008 to 2011, and is currently a Professor. His current research interests include power electronic control of electrical machines, electric/hybrid vehicle and ship drives, and power-converter circuits.